JOURNAL OF SPACECRAFT AND ROCKETS
Vol. 31, No. 2, March–April 1994

NASP Vehicle Interactions and Signatures above 100 Kilometers

B. David Green,* Girard A. Simons,† and Mark E. Fraser‡
Physical Sciences, Inc., Andover, Massachusetts 01810
and
Daniel Hastings§
Massachusetts Institute of Technology, Cambridge, Massachusetts 02139

As hypersonic space vehicles (such as the NASP X-30 Research Vehicle) traverse the 80–300 km altitude range, a variety of phenomena will arise from the interaction of the spacecraft with the residual atmosphere. Across this altitude regime, the flow surrounding the vehicle makes a transition from continuum to free molecular. A simple modeling effort is presented to quantify the variety of processes likely to occur. For example, communications will be severely hampered by the enhanced plasma cloud created at lower altitudes. Optical emissions will be generated in the high-velocity collisions of the atmospheric O, N_2, and O_2 with the vehicle surfaces and with outgassed molecules, transpired coolant, exhausts, and reflected atmospheric species. We have developed elementary gas kinetic descriptions of the flowfield and interaction lengths surrounding the lifting body vehicle. This information and assumed radiative efficiencies permitted predictions of relative radiance as a function of altitude. Quantitative predictions of the emissions from the ultraviolet through infrared spectral regions will occur and will result in decreased visibility of remote emission features. The local interaction radiances are sufficiently bright to obscure emission from the upper atmosphere and will even substantially obscure the hard Earth in certain bands.

Nomenclature

A	= sensor collection area, cm^2
$\bar{c}_e$	= emitted species thermal velocity, cm/s
e	= electron charge
f	= electromagnetic radiation frequency, Hz
M_∞	= freestream Mach number
m_e	= electron mass
$m(h)$	= Mach number as function of altitude
Nei	= photon collection rate, s^{-1}
n_e	= number density of emitted species, cm^3
n_i	= number density of incident species, cm^3
$p(h)$	= pressure as function of altitude, atm
q_{dynamic}	= dynamic pressure, atm
R	= radius of vehicle, cm
T	= temperature near surface of body, K
u_∞	= freestream velocity, 8 km/s
v	= vibrational quanta
γ	= specific heat ratio
λ_{ei}	= mean distance emitted species travels before striking incident species, cm
λ_{ie}	= mean distance incident species travels before colliding with emitted species, cm
πD^2	= collision cross section, cm^2
ρ/ρ_∞	= density ratio
ρ_e	= electron plasma density, cm^3
σ	= collision frequency, s^{-1}
Φ	= angle of attack, deg
Ω	= solid angle field of view, sr
ω_{pe}	= plasma frequency, Hz

Presented as Paper 91-0591 at the AIAA 29th Aerospace Sciences Meeting, Reno, NV, Jan. 7–10, 1991; received Oct. 15, 1991; revision received April 16, 1992; accepted for publication April 16, 1992.

*Vice President, Applied Sciences, 20 New England Business Center. Member AIAA.
†Principal Research Scientist, 20 New England Business Center. Member AIAA.
‡Principal Scientist, 20 New England Business Center.
§Associate Professor, Department of Aeronautics and Astronautics. Member AIAA.

Introduction

AS hypersonic space vehicles such as the National Aerospace Plane (NASP) X-30 Research Vehicle traverse the 80–300 km altitude range, a variety of phenomena will arise from the interaction of the space plane with the residual atmosphere. Across this altitude regime, the flow surrounding the vehicle makes a transition from continuum to free molecular. We present here a critical assessment of the phenomena that will result from this interaction to estimate their effect on communication and surveillance. Optical emissions will be generated in the high-velocity collisional interactions of the atmospheric O, N_2, and O_2 with the vehicle surfaces and with outgassed molecules, transpired coolant, exhausts, and reflected atmospheric species. We have used elementary kinetic theory to model the flowfield and interaction lengths surrounding a lifting hypersonic body. Over a range of assumptions of radiant efficiencies, both qualitative radiance predictions are made for a variety of scenarios. The near-field interaction radiances are sufficiently bright to obscure emission from remote objects in orbit and from the upper atmosphere. They will even substantially obscure the emissions from the solid Earth in certain bands. The wide range of plasma processes likely to be encountered are also considered.

Because of the desirability of using atmospheric O_2 as the oxidant, the NASP exit trajectory is planned to achieve near orbital velocity at altitudes with substantial atmospheric density. At 50-km altitude, velocities approaching 8 km/s, Mach 25 are achieved, and the vehicle pitches up and travels to higher altitudes. Greater surface heating rates are encountered on ascent than are expected for re-entry, which has a profile similar to that followed by the Shuttle. This trajectory poses severe demands on materials technology, the structure, cooling systems, aerodynamics, and the propulsion system.

We address the capabilities of the vehicle once it has arrived at cruise altitude in the low-density nonequilibrium upper atmosphere (thermosphere). At the lower end of this region, continuum flow is encountered, and a dense bow shock will exist in front of the plane that will generate a high degree of ionization and molecular dissociation and excitation. Above 100 km, flow is transitional to free molecular, and the atmosphere collides with the NASP vehicle and its effluent cloud at 8 km/s (Mach 25). Some data about orbital interactions at this altitude regime are provided by satellite and Shuttle observations, where optical emission glow is generated by collisions with the residual atmosphere, and plasma interactions create waves and noise. Orbital interaction optical emissions have

been observed between ~160 and 350 km in the uv, visible, and infrared spectral regions. They are believed to arise from many types of processes, including gas-phase collisions, material erosion, and surface-aided recombination. The on-orbit data clearly indicate emissions from N_2 and NO_2 electronic states and NO and OH vibrational emission.

We have assumed here that the NASP vehicle is moving at Mach 25 (orbital velocity) and is in a ballistic mode (i.e., that the main engines have shut down). We have examined steady-state cruise operation at a variety of altitudes both with hydrogen transpirational cooling and without. We have not addressed the variable effects of maneuvering thrusters (bipropellants, either H_2/O_2 or MMH/N_2O_4 systems) on the near-field vehicle environment. Our estimates of the flowfield are presented in the next section as a necessary basis for radiance and plasma predictions.

NASP Aerodynamics

The aerodynamics associated with the NASP vehicle are quite complex. It may operate as a jet, rocket, or orbiting vehicle withaltitude control rockets. Our intent here is to identify potential problems with surveillance and/or communication systems in a regime that has not been extensively studied with detailed computer codes. As such, we have concentrated on the high altitude (>100 km) regime where the ambient flowfield around the vehicle is in free molecular and transitional flow and the firing of the main or altitude engines would completely engulf the vehicle, leaving exhaust contaminants on the vehicle surface that may later be emitted.

The surface temperature of the NASP vehicle in *steady* flight will not exceed 1000 K above 100 km. Freestream molecules that strike the vehicle with velocity u_∞ (8 km/s) are fully or partially thermally accommodated at the vehicle surface and then leave the vehicle with thermal speed $\bar{c}_e \ll u_\infty$. This limit is termed "hyperthermal," and the hyperthermal mean free path completely characterizes the flowfield. This accommodation leads to the observed pressure enhancements over surfaces facing the velocity direction.

As shown in Fig. 1, incident molecules, velocity u_∞, and number density n_i strike a vehicle of radius R. They thermally accommodate at the vehicle's surface, leave with velocity $\bar{c}_e$ and number density n_e, and travel distance λ_{ei} (the hyperthermal mean free path) before striking another incoming molecule. The corresponding distance traveled by an incident species before striking an "emitted" (sub e) molecule is λ_{ie} whereas the mean free path between incident molecules is λ_{ii} (λ_∞) and that between emitted partners is λ_{ee}.

Elementary kinetic theory arguments[1] may be used to express λ_{ei} in terms of λ_∞ and the freestream Mach number M_∞ ($u_\infty/\bar{c}_\infty$):

$$\lambda_{ei} = \frac{\sqrt{2}\lambda_\infty(\bar{c}_e/\bar{c}_\infty)}{M_\infty} \ll \lambda_\infty \tag{1}$$

where $\bar{c}_\infty$ is the mean thermal speed in the incident flow. Note that λ_{ei} is much shorter than λ_∞ in the high Mach number ($M_\infty \gg 1$) or

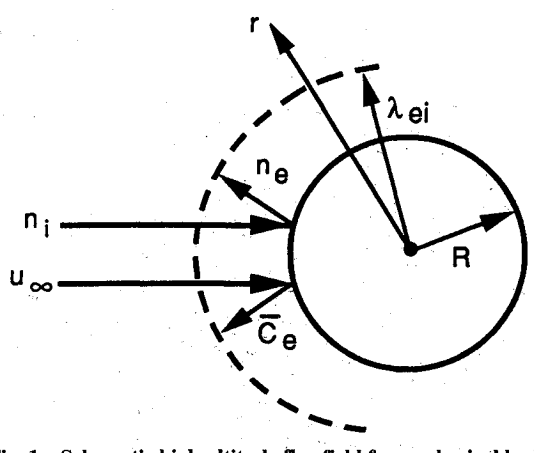

Fig. 1 Schematic high-altitude flowfield for a spherical body.

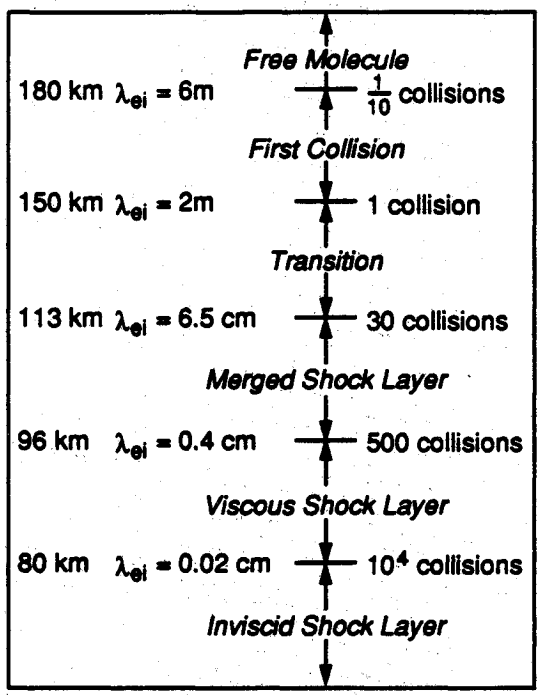

Fig. 2 NASP flow regimes (r = 2m, M_∞= 20).

hyperthermal limit ($u_\infty \gg \bar{c}_e$). This was first noted by Probstein[2] (λ_{ei} is ν_2 in his notation), and this distance has since been recognized as the critical hydrodynamic length scale since it is the shortest of the four length scales. These distances can be related through the hyperthermal mean free path as

$$\lambda_{ee} = \lambda_{ie} = \frac{r^2}{R^2}\lambda_{ei} \tag{2}$$

if an R^{-2} radial density falloff surrounding the body is assumed.

From the geometry illustrated in Fig. 1, it is clear that the fraction f of incident molecules scattered by e molecules is given by Eq. (3):

$$f = \frac{R^2}{\lambda_{ei}^2} \tag{3}$$

Free molecular flow is rigorous in the limit $f \to 0$. For all practical purposes, this regime is limited to $f < 0.1$ or $\lambda_{ei} > 3R$. A first collision regime is a perturbation to free molecule flow wherein each incident molecule suffers less than one collision, i.e., $f < 1$ or $\lambda_{ei} > R$. The transition flow then occurs for $f > 1$ or $R > \lambda_{ei}$.

Continuum descriptions of the flowfield are also quite diverse. At a low altitude, a distinct shock, an inviscid shock layer, and a boundary layer exist. At a higher altitude, the entire shock layer becomes viscous, but the shock wave and shock layer are distinct. At still higher altitudes, the shock and shock layer merge but possess sufficient (~30) collisions to justify use of the Navier-Stokes equations.

The sequence of flow regimes described earlier is illustrated in Fig. 2. Dominant gaseous radiation occurs in the hot inviscid shock layer with somewhat reduced signatures occurring in the cooler viscous shock layer. These regimes have been studied in detail with large hydro/radiation computer codes. The present effort concentrates on the higher altitudes where rarefied flow models are required.

In the free molecular and first collision regimes, the e-i collisions dominate over the length scale λ_{ei}, and the associated collision frequency σ_{ei} is greater than that of the other collisions. However, in the transition regime, all collisions are equally probable and occur on the same length scale λ_{ei}. Simplified models for these flowfields have been generated[1] and used to predict radiation signatures seen by an on-board sensor with collection area A and solid angle field of view Ω. If each e-i collision produces N_{ei} photons in

a spectral bandpass of interest, the net photon collection rate at the sensor becomes

$$\dot{N}_{ei} = \frac{N_{ei}\Omega A \bar{c}_e}{(4\pi R)\,\pi D^2}\left[\left(\frac{R^2}{\lambda_{ei}^2}\right)e^{-R/\lambda_{ei}}\right] \tag{4}$$

where πD^2 is the collision cross section of the *e-i* collision. The rightmost term, denoted [ ] hereafter, contains the altitude dependence of $\dot{N}_{ei}$.

Following a similar exercise for *e-e* collisions, we assume each *e-e* collision produces N_{ee} photons and the photon count on the detector assumes the same form, with $\dot{N}_{ee}$ replacing N_{ei} and the altitude dependence [ ] is

$$[\,] = \frac{1}{3}\frac{R^2}{\lambda_{ei}^2} \tag{5}$$

in free molecule flow and

$$[\,] = \frac{1}{2}\frac{R}{\lambda_{ei}} \tag{6}$$

in the transition regime.

Applying this model to the NASP lifting underbody, shown in Fig. 3, at angle of attack Φ, now results in a $1/r$ scaling of the emitted density ne. The dominant relative effect is that $\dot{N}_{ei}$ is reduced by $\sin\Phi$, $\dot{N}_{ei}$ is reduced by $\sin\Phi$, and $\dot{N}_{ee}$ is reduced by $\sin^2\Phi$.

These results are illustrated in Fig. 4 for a 2-m radius body. The previous treatment applies only to the highest altitudes where R/λ_{ei} is less than 0.3 (and could possibly be extrapolated to the first collision limit of $R/\lambda_{ei} < 1$). The N_{ei} continues to increase with decreasing altitude and peaks in the transition regime, where each incident molecule strikes at least one emitted molecule. At altitudes below 150 km, self-collisions separate the incident and emitted molecules. Collisions between emitted species are less energetic than *e-i* collisions and closer to the energetic threshold for excitation. We have assumed photon yields for *e-e* collisions as an order of magnitude lower than for *e-i* collisions. Nevertheless, as altitude decreases below 150 km, the number of *e-e* collisions grows until they dominate the radiation signature in the merged layer. This emission continues to increase in the viscous and inviscid shock layer regimes.

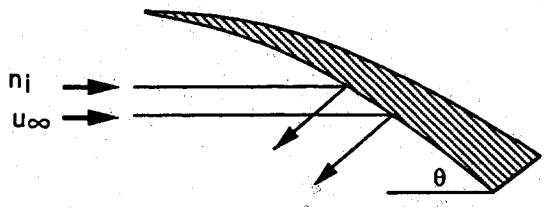

Fig. 3 Schematic high-altitude flowfield for a lifting NASP body.

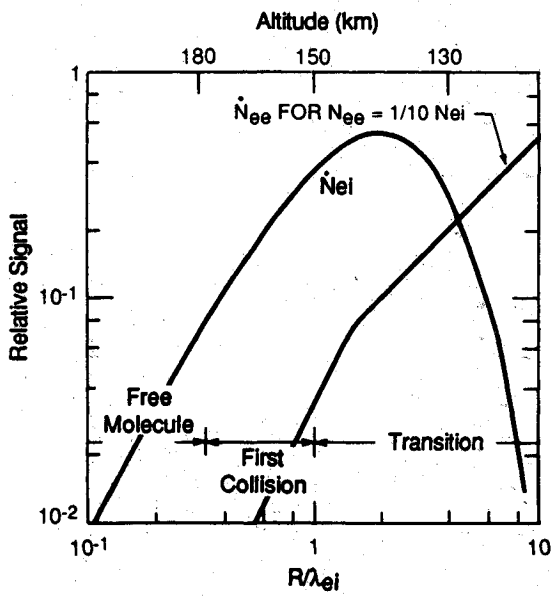

Fig. 4 Radiation in the rarefied flow regime ($R = Z_m$, $M_\infty = 20$).

Potential Optical Sensor Interferences for NASP

The impact of high-velocity atoms and molecules will produce a near-field glow that may interfere with sensor performance. Although poorly understood, these glows have been observed on the Shuttle and various satellites. A recent summary of the observations is provided by Garrett et al.[3] We present a preliminary estimate of the magnitude of the near-field glows covering the wavelength range of 0.1–100 μm for the vehicle at 100 and 300 km altitudes. We have compared the results of our glow calculations with various backgrounds and anticipated operational signatures. The backgrounds are the hard Earth signature (reflected Sun and Earth shine) and Earth limb dayglow/nightglow. The operational scenario examined is the tracking of blackbodies (300 and 2000 K). A functional NASP will have to avoid or track other objects in low-Earth orbit (LEO).

To estimate the near-field glow, we have considered gas-phase reactions, surface reactions, collisional excitation processes, and direct $T \rightarrow E$, v processes (conversion of collisional momentum into electronic or vibrational excitation). The methodology employed is similar to previous studies of glow we have performed for the Space Station and for smaller LEO vehicles.[4,5] We have used experimental data wherever possible and reasonable estimates where data are unavailable.

The first scenario we consider is with H_2 transpirant on to cool the vehicle after its ascent. The surface temperatures are assumed to be ~1800 K just after completing ascent, higher than the steady operational value of 1000 K.

The transpirant flow (number densities as high as 10^{14} H_2 molecules cm^{-3} above NASP surfaces) creates a multicollisional regime such that all incoming atoms and molecules are accommodated at all altitudes, and the collisional regimes of Fig. 4 do not apply. Therefore, only thermalized species will interact with NASP surfaces.

The important excitation reactions for the transpirant-on case are gas-phase (emitted-emitted) interactions producing OH(v),[6–8]

$$H_2(v \geq 1) + O \rightarrow OH(v = 1) + H \tag{7}$$

$$H + O_2 \rightarrow OH(v = 1) + O \tag{8}$$

reactions of vaporized Aℓ and Ti atoms from the titanium aluminide surface,[9]

$$A\ell + O_2 \rightarrow A\ell O(B, X, v) + O \tag{9}$$

$$Ti + O_2 \rightarrow TiO(X, v) + O \tag{10}$$

and surface reactions of chemisorbed H and O to produce vibrationally excited OH and H_2O,

$$H_{ads} + O_{ads} \rightarrow OH(v) \tag{11a}$$

$$\rightarrow H_2O(\nu_1, \nu_2, \nu_3) \tag{11b}$$

These surface catalyzed and gas-phase chemiluminescent oxidation reactions will dominate the signature in this scenario.

Collisional excitation processes will not contribute to the signature since most of the collisions are between infrared inactive homonuclear diatomics and atoms. Because all of the incoming O and O_2 flux is consumed by H and H_2 reactions, other surface reactions to form NO do not occur at an appreciable rate. We have not included the collisional vibrational excitation of H_2. If the cross section for this process is as high as 10^{-17} cm^2, then the concentration of $H_2(v)$ would be enhanced by an order of magnitude over our thermal equilibrium values. Because of a lack of experimental or

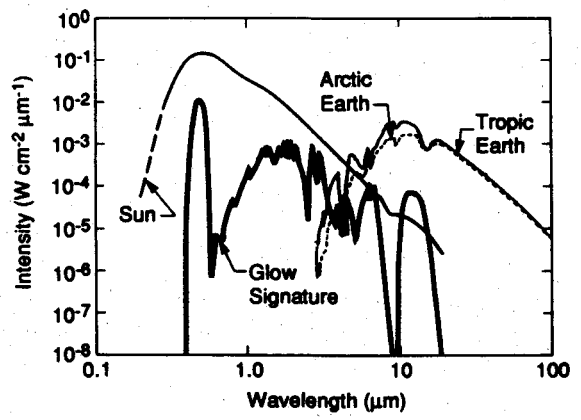

Fig. 5 Predicted NASP glow signature at 100 km, transpirant on in comparison with hard Earth signature.

theoretical determinations of this cross section, we have not included this last process in our signature estimates.

The second scenario we consider is with transpirant off and all hydrogen thoroughly outgassed from NASP surfaces, and the surfaces are assumed to be cool. At low altitudes, a multicollisional regime is established by rebounding atmospheric species. Emitted-emitted and surface processes dominate the signature as expected from Fig. 4. At 300-km altitudes, the flow will be free molecular and the incoming flux will not be accommodated before colliding with the surfaces. Incident-emitted interactions will dominate the signature.

Surface reactions producing NO and NO_2 will dominate the observed glow for this scenario,

$$N_{ads} + O_{ads} \rightarrow NO(v) \tag{12a}$$

$$NO_{ads} + O \rightarrow NO_2(\nu_2, \nu_3) \tag{12b}$$

$$\rightarrow NO_2(E) \tag{12c}$$

where E represents electronic excitation. These interactions will occur between dissociatively chemisorbed N_2 and O_2. We have used dissociation efficiencies of 10^{-3} and 10^{-1} for N_2 and O_2, respectively. These values are consistent with metals such as tungsten.[10]

Another surface reaction that must be considered is the one that is responsible for $N_2(a - x)$ LBH emissions. These bands have been directly observed above several vehicle surfaces over the 180–240 km regime. Sufficient data have been obtained for an atmospheric density scaling of the intensity to be determined.[11] The dependence has been found to be cubic, either cubic in N_2 or squared in N_2 and first power in O_2. This source of glow has been added to our estimates by scaling the literature observations. With this altitude scaling, emission from these features is not significant above 240 km.

Spectral Predictions

Glow spectra have been calculated for transpirant-on and -off scenarios at altitudes of 100 and 300 km. To assess the effect of these glows on sensor performance, we now compare these results with the background and operational scenarios. Figure 5 shows the interaction signature with the transpirant on at 100 km in comparison with the hard Earth spectrum. These emissions will be observed if NASP sensors look directly down during the daytime. With the exception of looking directly at the Sun, this is the brightest background to be encountered. The predicted glow spectrum for transpirant on at 100 km is substantial, nearly equal in magnitude to the hard Earth spectrum over most wavelengths. The brightest features are due to OH and AℓO vibrational bands in the infrared and AℓO(B-X) in the visible. For 300 km the transpirant-on predicted glow decreases by about 10^3 for the features dependent on O atoms (e.g., OH) and 10^6 for features dependent upon O_2 (e.g., AℓO).

To properly function, NASP sensor systems must be able to properly target far-field objects for collision avoidance. Figures 6 and 7 show the predicted spectra in comparison with 300 and 2000 K blackbodies. The 300 K blackbody has been taken to be 100 km distant. We have also included a component for reflected sunlight. The 2000 K blackbody is also for 100 km distance but for a larger vehicle. Figure 6 shows the blackbody spectra in comparison with the 300 km transpirant-on data. This comparison shows that the vehicle near-field glow will exceed the 300 K blackbody signal for all wavelengths for which we have calculated glow. The near-field glow is equivalent to the 2000 K blackbody signal. The results for 100 km altitude transpirant on exceed those for 300 km by 10^3 to 10^6. Thus, at 100 km altitude the vehicle glow will exceed even the brightest blackbody. Clearly, optical observations will be severely compromised while transpirational cooling is ongoing.

The optical environment is considerably improved when the transpirant, hydrogen, is off. At 300 km the transpirant-off glow exceeds 300 K blackbody emission at several wavelengths but is well below the signal level for the 2000 K body. At 100 km, however, the glow signature equals or exceeds the 2000 K body at most wavelengths as displayed in Fig. 7.

The radiance predictions presented in this section indicate substantial optical interference during both transpirant-on and transpirant-off scenarios, particularly at lower altitudes. In many wavelengths, we predict that the near-field emissions will equal or exceed the signals from the considered targets and backgrounds.

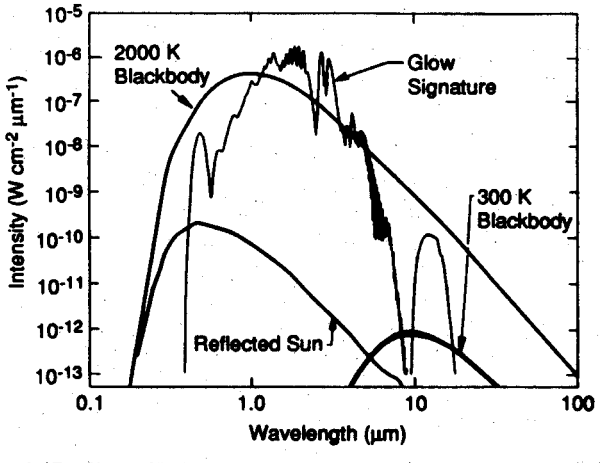

Fig. 6 Predicted NASP glow signature at 100 km, transpirant on in comparison with 300 and 2000 k, 100 km distant blackbodies.

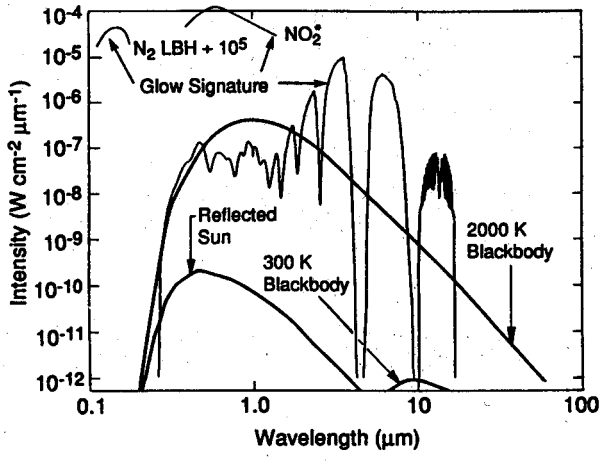

Fig. 7 Predicted NASP glow signature at 100 km, transpirant off in comparison with 300 and 2000 k, 100 km distant blackbodies.

Table 1 Electromagnetic bands

Band	Frequency, GHz	Plasma density, m^{-3}
Vlf	$3–30\times10^{-6}$	$1.12–112\times10^{5}$
Vhf	$30–30''\times10^{-\times}$	$1.12–112\times10^{13}$
Uhf	0.3–3	$1.12–112\times10^{15}$
S	2.6–3.95	$8.4–19.4\times10^{16}$
X	8.2–12.4	$8.37–19.13\times10^{17}$
K	18–26.5	$4.03–8.73\times10^{18}$
Infrared	3,000–430,000	$1.12–22.985\times10^{23}$

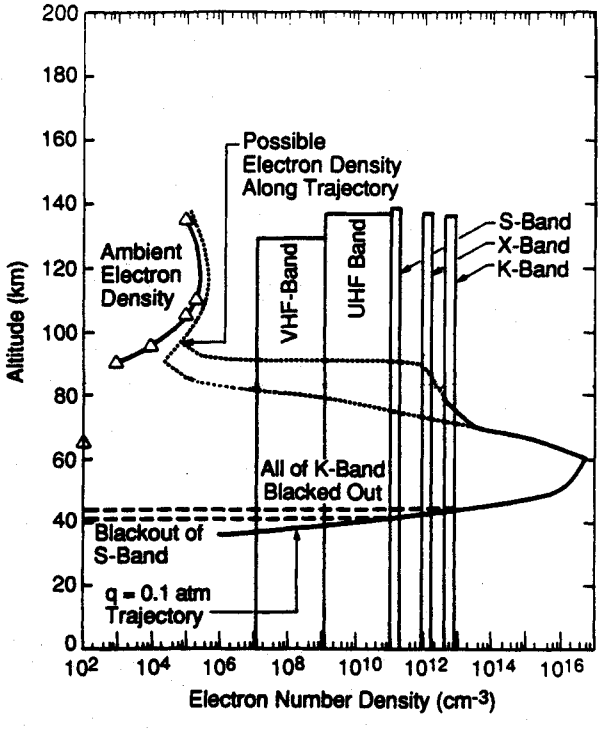

Fig. 8 Electron density as a function of altitude upon ascent.

Influence of Plasma Effects on Hypersonic Vehicles

During ascent the hypersonic vehicle will have a plasma sheath surrounding it (similar to that around a re-entry body). Once on orbit, it will be subject to a number of plasma interactions between its own self-generated plasma and the environment.

Vehicles re-entering the atmosphere of the Earth undergo a "blackout" period[12] when the local plasma density around the body rises to a level that reflects waves in the microwave range, preventing communication with the vehicle. This typically occurs in the 30–60 km altitude range as the vehicle is rapidly slowing from orbital velocities. This effect is well understood for altitudes up to approximately 100 km. The flowfield about the body is continuum flow, and the air is shock heated over the surface of the body to produce the plasma layer that reflects the radio waves. The formation of a disruptive plasma layer over portions of the body is less well understood for altitudes above 100 km and for flight over the polar caps.

For reference in the following sections, we define the range of electromagnetic frequencies and the associated plasma density in Table 1. The plasma density is defined through the relation

$$2\pi f = \omega_{p_e} = \sqrt{\frac{e^2 \rho e}{m_e \varepsilon_0}} \tag{13}$$

where f is the frequency of the electromagnetic radiation.

On ascent a hypersonic vehicle must operate on a trajectory satisfying the twin constraints of having sufficient dynamic pressure to drive the combustion process while keeping the heat flux from the shock-heated air at an acceptable level. We have considered a trajectory through the atmosphere with a constant dynamic pressure.

The Mach number at altitude h was obtained from

$$M(h) = \sqrt{\frac{2q_{\text{dynamic}}}{\gamma p(h)}} \tag{14}$$

where $\gamma=1.4$. The dynamic pressure q_{dynamic} required to operate the scramjet was taken as 0.1 atm. The pressure and the mean free path between collisions at a given given altitude are from the U.S. Standard Atmosphere.[13] A constant dynamic pressure can be maintained up to approximately 60 km altitude, when a "pop-up" maneuver would be performed.

The temperature near the surface of the body is taken to be the stagnation temperature,

$$T = T_{\text{ambient}}\left[1 + {}^1\!/_2\,(\gamma - 1)\,M^2(h)\right] \tag{15}$$

The density ratio ρ/ρ_∞ in the continuum range is obtained from the well-known normal shock relations $\rho/\rho_\infty=(\gamma+1)M^2/[(\lambda-1)M^2+2]$. The variables ρ_∞ and T_{ambient} are obtained from the U.S. Standard Atmosphere.[13] Once we have T and the ratio ρ/ρ_0 (ρ_0 is the density at sea level), then we can use the equilibrium electron density graphs in Martin.[12] These graphs relate ρ_e to ρ/ρ_0 with T as a parameter. Use of the Rankine-Hugoniot relationship for ρ/ρ_0 is only valid in the continuum limit.

The calculated electron number density is shown as a function of altitude in Fig. 8. The plotted curves are obtained from a continuum, equilibrium approach and should be regarded as most accurate at the lower altitudes. Also shown is the ambient electron number density. This is seen to be very small. Above altitudes of 35 km, the electron density over the surface of the body rises extremely rapidly. Just above 40 km, S-band communications would be blocked out for antennas near the leading edge of the body. By an altitude of 46 km, all communications through the K-band would be blocked. At the highest altitude accessible with the scramjet (60 km), the electron density would rise to the 10^{16} cm^{-3} level. At altitudes above 60 km, the electron density will drop rapidly to ambient. Hence, for a trajectory of $q_{\text{dynamic}}=0.1$ atm, there will be considerable electromagnetic interference between 40 and approximately 80 km in altitude. Above this altitude, the electron density will be too small to block communications, although some modification could occur.

The situation for altitudes in the 100-km range is even more complex. The flow around the body is in the transitional regime ($f > 1$), and a shock-heated air layer cannot form. Thus, the plasma sheath arising from ionization of the air is not expected. However, the vehicle may be actively emitting various types of neutral gases. On the ascent trajectory, the vehicle will actively cool itself by transpiring hydrogen even after it arrives at cruise altitudes. In addition, if the vehicle uses attitude control thrusters, it will produce gases like carbon dioxide and water in the vicinity of the vehicle. At altitudes of 240–300 km, an enhanced plasma cloud was observed around the Shuttle orbiters that arises from emitted gases such as water and carbon dioxide. These gases undergo charge exchange with the ambient oxygen, creating a local plasma. At 300-km altitudes, this plasma cloud will stay with the vehicle for a substantial period of time[14] through a complex electrodynamic interaction with the Earth's magnetic field. Observations from the Shuttle indicate that local plasma densities up to an order of magnitude above the ambient occur. This enhancement cannot produce cutoff of the radio signals in the microwave bands.

Chemical equilibrium calculations of the plasma density[12] expected in the Earth's atmosphere at 120 km around a body moving at 7 km/s indicate a density on the order of 10^{15} m^{-3}. This will give a cutoff frequency of 684 MHz, which is in the uhf band. Disruption of communication frequencies in the microwave band will occur only if the gas density surrounding the vehicle substantially exceeds ambient and an additional ionization process occurs.

In polar orbits this neutral cloud around the vehicle will partially ionize upon transit through the auroral oval due to the bombardment by high-energy electrons. Even an optimistic estimate gives a plasma density that is considerably enhanced above ambient but not sufficient to block or even significantly modify microwave communications. Data from polar orbiting satellites indicate that on occasion the vehicle may charge to a large negative potential.[15] This will occur if it is struck by a high-energy auroral stream at the same time as it passes through an ion hole. If this occurs, then classical Paschen breakdown may occur on the surface of the vehicle. These discharges could damage the vehicle's surface material. These occasions will be rare for operational NASP scenarios.

Conclusions

We have addressed the ability of the future NASP research vehicle to perform remote observations when operating in a high-altitude (above 80 km) cruise mode. The NASP vehicle will encounter a variety of flow regimes on ascent, from inviscid to viscous to merged shock layers (80 to 110 km), then transitional to first collision, and finally free molecular above 180 km. The vehicle will be actively cooled by H_2 transpiration on ascent and initially at cruise altitudes. Thus, a variety of interaction length scales will be encountered for both incident, reflected, and surface-produced species. These interactions have been assessed through our flow modeling. It created a framework for considering the role of high-velocity interactions with the atmosphere and redistribution of the collision kinetic energy into chemical reactions, ionization, and optical emissions. We then made radiance predictions based on estimates of collision cross sections. In addition, spectra of the interactions were modeled and compared with remote observables such as the hard Earth, another space vehicle, and the Earth's upper atmosphere.

Although not covered in this paper, the variability of the local environment must be addressed in future studies. The main engine and maneuvering thrusters will generate plumes large enough to engulf the entire vehicle, contaminating its surfaces. This surface contamination can create additional near-field optical emissions long after the plume has been swept away.

Substantial optical emissions are observed both with and without H_2 transpiration cooling. At an altitude of 100 km, with the transpirant on, the near-field SWIR and MWIR radiances rival Earth emission/reflection, compromising observations. The near-field signature at this altitude also dominates the detected far-field radiance arising from boost phase vehicles or other on-orbit spacecraft at most wavelengths across the spectrum. At an altitude of 300 km, spacecraft detection is still compromised in the infrared, and the emission from the Earth's upper atmosphere is obscured particularly in low emission "window" regions.

A broad range of plasma processes will be occurring over the vehicle's surfaces. On ascent, a communications blackout will be in effect from 40 to 80 km. During cruise operation above these altitudes, activities should not hamper communication. However, a variety of phenomena such as surface discharges or enhanced ionization are expected around the auroral oval.

Acknowledgments

This effort was supported by the National Aerospace Plane Joint Program Office as part of the Small Business Innovative Research Program. The authors benefited from many useful discussions with David Cooke and Charles Pike of the Phillips Laboratory. Alan Gelb of Physical Sciences, Inc., assisted in the chemical reaction analysis. The authors also acknowledge the assistance of the reviewers in improving this paper.

References

[1]Green, B. D., Fraser, M. E., Simons, G. A., Hastings, D., and Gelb, A., "Hyper Space Vehicle Interactions and Signature," Physical Sciences, Inc., PSI-2104/TR-1003, Andover, MA, Feb. 1990.

[2]Probstein, R. F., "Shock Wave and Flowfield Development in Hypersonic Reentry," *ARS Journal,* Vol. 31, 1961, pp.185–194.

[3]Garrett, H. B., Chutjian, A., and Gabriel, S., "Space Vehicle Glow and Its Impact on Spacecraft Systems," *Journal of Spacecraft and Rockets,* Vol. 25, No. 5, 1988, pp. 321–340.

[4]Fraser, M. E., Gelb, A., Green, B. D., and Torr, D. G., "Calculation of Space Station Infrared Irradiance from Atmosphere-Induced Emissions," *A Study of Space Station Contamination Effects,* NASA Conf. Publication 3002, Oct. 1988, pp. 62–69.

[5]Gelb, A., and Fraser, M. E., "Interceptor Blinding from Atmospheric-Induced Emissions," Physical Sciences, Inc., PSI-391/TR-564, Final Rept., Defense Nuclear Agency Contract DNA001-85-C-0391, Andover, MA, April 1986.

[6]Broida, M., and Persky, A., "Quasiclassical Trajectory Study of the Reaction $O(^3P)+H_2 \rightarrow OH+H$. The Effects of the Location of the Potential Energy Barrier, Vibrational Excitation and Isotopic Substitution on the Dynamics," *Journal of Chemical Physics,* Vol. 80, No. 8, 1984, pp. 3687–3695.

[7]Joseph, T., Truhlar, D. G., and Garrett, B. C., "Improved Potential Energy Surfaces for the Reaction $O(^3P)+H_2 \rightarrow OH+H$," *Journal of Chemical Physics,* Vol. 88, No. 10, 1988, pp. 6982–6990.

[8]Miller, J. A., "Collision Dynamics and the Thermal Rate Coefficient for the Reaction $H+O_2 \rightarrow OH+O$," *Journal of Chemical Physics,* Vol. 74, No. 9, 1981, pp. 5120–5132.

[9]Fontijn, A., and Felder, W., "High Temperature Flow Tubes; Generation and Measurement of Refractory Species," *Reactive Intermediates in the Gas Phase,* Academic, New York, 1979, pp. 59–149.

[10]Auerbach, D. J., Pfnür, H. E., Rettner, C. T., Sclagegel, J. E., Lee, J., and Madix, R. J., "Kinetic Energy and Angular Dependence of Activated Dissociative Adsorption of N_2 on W(110): Observed Insensitivity to Incidence Angle," *Journal of Chemical Physics,* Vol. 81, No. 5, 1984, pp. 2515, 2516.

[11]Conway, R. R., Meier, R. R., Strobel, D. F., and Huffman, R. E., "The Far Ultraviolet Vehicle Glow of the S3-4 Satellite," *Geophysics Research Letters,* Vol. 14, No. 6, 1987, pp. 628–631.

[12]Martin, J. J., *Atmospheric Reentry: An Introduction to Its Science and Engineering,* Prentice-Hall, Englewood Cliffs, NJ, 1966.

[13]Anon., *U.S. Standard Atmosphere,* NOAA, NASA, and U.S. Air Force, Washington, DC, 1976.

[14]Caledonia, G. E., Person, J. C., and Hastings, D. E., "The Interpretation of Space Shuttle Measurements of Ionic Species," *Journal of Geophysical Research,* Vol. 92, Jan. 1987, pp. 273–281.

[15]Yeh, H.-C., and Gussenhoven, M. S., "The Statistical Electron Environment for Defense Meteorological Satellite Program Eclipse Charging," *Journal of Geophysical Research,* Vol. 92, July 1987, pp. 7705–7715.

Ernest V. Zoby
Associate Editor